Journal of Magnetism and Magnetic Materials 591 (2024) 171701

Contents lists available at ScienceDirect

Journal of Magnetism and Magnetic Materials

journal homepage: www.elsevier.com/locate/jmmm

Research article

Magnetically driven confined colloids: From enhanced diffusion to bidirectional transport

Mattia Ostinato [a,b], Antonio Ortiz-Ambriz [c], Pietro Tierno [a,b,d,*]

[a] Departament de Físca de la Matèria Condensada, Universitat de Barcelona, Martí i franques 1, Barcelona, 08028, Spain
[b] Universitat de Barcelona Institute of Complex Systems (UBICS), Universitat de Barcelona, Martí i franques 1, Barcelona, 08028, Spain
[c] Tecnológico de Monterrey, School of Engineering and Sciences, Ave. Eugenio Garza Sada 2501, Monterrey, 64849, Mexico
[d] Institut de Nanociència i Nanotecnologia, Universitat de Barcelona, Martí i franques 1, Barcelona, 08028, Spain

ARTICLE INFO

Keywords:
Magnetic colloids
Microscale transport
Diffusion

ABSTRACT

Inspired by previous experimental results, we use numerical simulations to investigate the collective dynamics of paramagnetic colloidal particles confined between two plates closer than twice the particle diameter and driven by an external precessing magnetic field. We show that, when the field is spatially isotropic there is no net particle current and the colloids display enhanced diffusive dynamics with an effective diffusion coefficient which raises up to 60 times that of the undriven case. In contrast, when the field is spatially anisotropic due to a small tilt angle δ, the particles organize into a robust bidirectional current, flowing along two parallel planes by periodically exchanging their positions. In this regime, we also analyze how the presence of small impurities which can be described as "magnetic holes" affect the particle current breaking the bidirectional flow. Our system provides a general method to transport magnetic colloids in a viscous fluid, without using any field gradient, but based on the fine balance between confinement and magnetic dipolar interactions.

1. Introduction

The transport of microscale particles in fluid media is appealing since it reveals novel physical mechanisms [1,2] and it is also directly related to technological applications in microfluidic systems [3]. The understanding of how microscopic particles move and interact when subjected to external fields may shed light on the dynamics of similar transport phenomena on different length scales, such as pinning–depinning transitions [4,5], friction [6,7], synchronization [8,9] or directional locking effects [10–12]. These particles can also be used to measure the resistance and interactions mediated by the dispersing medium, e.g. the hydrodynamic one, and thus represent a simplified model system for biological entities such as bacteria, that are characterized by similar length scales [13–16]. From the technological side, colloidal particles can be chemically functionalized such that they can bind to biological or chemical cargoes and act as field controllable drug delivery vectors. Thus, these particles have potential application in the controlled delivery of chemicals or drugs within microfluidic networks [17–19].

Magnetic colloids such as polystyrene particles doped with iron oxide grains, can be manipulated in a fluid via external magnetic fields. The usual strategy to transport these particles is the magnetophoresis [20,21], where colloids move in response to an external field gradient [22]. The inhomogeneous field can be generated either from a localized source such as a permanent magnet [23,24], or due to magnetizable patterns [25–29]. As an alternative method, recently [30,31] we reported the possibility of moving magnetic colloids by using a combination of strong confinement and magnetic dipolar interactions. This transport mechanism was triggered by an homogeneous time-dependent field and the particles located close to the confining walls were able to exchange position continuously performing a "ceilidh"-like dance.

Here we provide detailed numerical simulations of this system and show that, when the applied precessing field is spatially isotropic, the driven particles display enhanced diffusive dynamics for a given range of field parameters. In contrast, using a small spatial asymmetry created by adding an additional bias, we find that the particles organize into a bi-directional current where colloids located in the upper plane slide across particles close to the bottom substrate in a continuous way. In this exchange process, we show that the particle current is rather robust independently from the presence of defects in the form of unpaired dimers, but it can be easily destabilized when "magnetic holes" are introduced.

* Corresponding author at: Departament de Físca de la Matèria Condensada, Universitat de Barcelona, Martí i franques 1, Barcelona, 08028, Spain.
E-mail address: ptierno@ub.edu (P. Tierno).

https://doi.org/10.1016/j.jmmm.2023.171701
Received 26 October 2023; Received in revised form 28 December 2023; Accepted 29 December 2023
Available online 2 January 2024

2. Brownian dynamics

We consider $i = 1...N$ paramagnetic colloidal particles with diameter d and located at position $\boldsymbol{r}_i = (x_i, y_i, z_i)$ within a box of sizes $L_x \times L_y \times h$. We impose periodic boundary conditions on the $(\hat{\boldsymbol{x}}, \hat{\boldsymbol{y}})$ plane and place two hard walls along the $\hat{\boldsymbol{z}}$ axis at positions $z = \pm\frac{h}{2}$. For each particle i we integrate the overdamped equations of motion:

$$\gamma \frac{d\boldsymbol{r}_i}{dt} = \sum_{j \neq i} \boldsymbol{F}_{int}(\boldsymbol{r}_i - \boldsymbol{r}_j) + \boldsymbol{F}_w + \boldsymbol{F}_g + \boldsymbol{\eta}(t) \ , \tag{1}$$

being γ the friction coefficient. The total force exerted on particle i by particle j is given by, $\boldsymbol{F}_{int}(\boldsymbol{r}_i - \boldsymbol{r}_j) = -\nabla U_{int}(\boldsymbol{r}_i - \boldsymbol{r}_j)$, where $U_{int}(\boldsymbol{r}_i - \boldsymbol{r}_j) = U_{\rm dip}(\boldsymbol{r}_i - \boldsymbol{r}_j) + U_{WCA}\left(\left|\boldsymbol{r}_i - \boldsymbol{r}_j\right|\right)$. In this equation, $U_{\rm dip}$ is the magnetic dipolar interaction, that for two particles (i, j) with magnetic dipole moments $\boldsymbol{m}_{i,j}$ and at a relative distance $r = |\boldsymbol{r}_i - \boldsymbol{r}_j|$ can be written as,

$$U_{dip} = -\frac{\mu_0}{4\pi r^5}\left[3(\boldsymbol{m}_i \cdot \boldsymbol{r})(\boldsymbol{m}_j \cdot \boldsymbol{r}) - (\boldsymbol{m}_i \cdot \boldsymbol{m}_j)r^2\right] \ , \tag{2}$$

being $\mu_0 = 4\pi \times 10^{-7}$ H m^{-1} the vacuum permeability (similar to that of water). Moreover, U_{WCA} is a repulsive Weeks–Chandler–Andersen (WCA) potential which is given by,

$$U_{WCA} = \begin{cases} 4\epsilon\left[\left(\frac{d}{r}\right)^{12} - \left(\frac{d}{r}\right)^{6}\right] + \epsilon & \text{for } r < 2^{\frac{1}{6}} d \\ 0 & \text{for } r > 2^{\frac{1}{6}} d \end{cases} \tag{3}$$

This potential is also used to model the force $\boldsymbol{F}_w$ exerted by the confining walls on particle i, while $\boldsymbol{F}_g = -\Delta\rho V g \hat{\boldsymbol{z}}$ is the gravitational force being $\Delta\rho = \rho_p - \rho_w$ the density mismatch between the particle of volume $V = \pi d^3/6$ and the surrounding fluid, in this case water. The thermal noise is given by the term $\boldsymbol{\eta}(t) \equiv (\eta_x, \eta_y, \eta_z)$ where each random Gaussian variable has zero mean, $\langle \eta_i(t) \rangle = 0$ and is delta correlated, $\langle \eta_i(t)\eta_j(t') \rangle = 2k_B T\gamma\delta_{ij}\delta(t - t')$, being T the thermodynamic temperature and k_B the Boltzmann constant.

In our numerical simulations we use the free package LAMMPS [32] that was home modified in order to include an overdamped integrator and the particles' induced dipole moment. As parameters for our simulations we use values similar to the experimental ones reported in Ref. [30] with $d = 2.8$ μm, $\gamma = 56.75 \times 10^{-6}$ pN s nm^{-1}, $\Delta\rho = 10^3$ kg m^{-3}, $h = 3.9$ μm, $B_0 = 7.28$ mT, $\theta = 27°$, $T = 300$ K and use as energy scale for the WCA potential $\epsilon = 10^4$ pN nm. We point out that with this choice of parameters the distance between the confining walls is such that $h < 2d$, so that two particles cannot slide one on top of the other. This set of values is used for most of the simulations except for the unbiased case, where we observed the enhanced diffusive dynamics. Here we have switched off the gravitational force, thus placing $\Delta\rho = 0$ and used a similar value for the friction coefficient, $\gamma = 59.17 \times 10^{-6}$ pN s nm^{-1}, which was previously [30] obtained from the measured diffusion coefficient of a paramagnetic particle performing free diffusion.

Depending on the phenomenon to investigate, the simulations start with either particles randomly arranged in the $z = 0$ plane, or with particles arranged in pre-formed dimers in the $z = 0$ plane, such that the centers of mass of these dimers form a triangular lattice. This initial condition allows us to start from a situation where every particle already has a neighbor, giving us a clearer picture of some of the regimes investigated in this paper. In each section we will specify the initial conditions used as well as the normalized particle packing fraction, defined as $\Psi = N\pi d^2/(4A)$, being A the total area considered that encloses the N particles. All simulations are run by integrating Eq. (1) with a time step of $\Delta t = 10^{-4}$ s.

3. Confined paramagnetic colloids

Fig. 1 illustrates a sequence of experimental images adapted from a previous work [30], showing the collective organization of a strongly confined ($h = 3.9$ μm) collection of paramagnetic colloidal particles under a time dependent magnetic field. The particles used in these experiments and in the current simulations are paramagnetic colloids of diameter $d = 2.8$ μm and magnetic volume susceptibility $\chi = 0.4$. In presence of an external magnetic field $\boldsymbol{B}$, a free particle acquires a dipole moment $\boldsymbol{m} = V\chi\boldsymbol{B}/\mu_0$ that points along the field direction. When considering several particles, we neglect effects due to depolarization given the low strengths of the applied field [33], and also take into account the mutual induction between different dipoles [34]. Thus, each particle i acquires a non-saturated dipole moment $\boldsymbol{m}_i = (V\chi/\mu_0)(\boldsymbol{B} + \boldsymbol{B}_{ind}(\boldsymbol{r}_i))$, and the mutual induction is considered by the term

$$\boldsymbol{B}_{ind}(\boldsymbol{r}_i) = \sum_{j \neq i} \frac{\mu_0}{4\pi r_{ij}^3}\left[\frac{3(\boldsymbol{m}_j \cdot \boldsymbol{r}_{ij})\boldsymbol{r}_{ij}}{r_{ij}^2} - \boldsymbol{m}_j\right] \ , \tag{4}$$

which represents the magnetic field induced at the position of particle i by the magnetic moments of the other colloids, while $\boldsymbol{r}_{ij}$ is the distance between particles i and j. In particular, $\boldsymbol{m}_i$ and Eq. (4) are evaluated iteratively, with a number of iterations that we calibrated to stabilize the dipole moments. Thus, pairs of particles experience long-range dipolar interactions, apart from excluded volume at short distances. In particular, Eq. (2) shows that via an applied field $\boldsymbol{B}$ one can tune these interactions from attractive to repulsive depending on whether the particles induced moments $\boldsymbol{m}_{i,j}$ are parallel or perpendicular to the vector joining their centers $\boldsymbol{r}$, respectively.

Compared to previous works where these particles were subjected to static fields [35–37], our system shows two additional features. First, we use a strong confinement with a cell of thickness $h < 2d$, such that two particles may only pass each other by moving along the $(\hat{\boldsymbol{x}}, \hat{\boldsymbol{y}})$ plane, not perpendicular to it, bottom of Fig. 1(a). It was previously shown that, under this condition, a static field perpendicular to the confining plane, could induce a wide variety of self-assembled structures characterized by hexagonal, square, stripe or labyrinth-like ordering [38]. Indeed the confinement "softens" the pair repulsion with respect to the case of particles fully squeezed in the $(\hat{\boldsymbol{x}}, \hat{\boldsymbol{y}})$ plane, where Eq. (2) assumes the form $U_{dip} = (\mu_0 m^2)/(4\pi r_{\parallel}^3)$. Indeed, when subjected to a field along the $\hat{\boldsymbol{z}}$ direction, Eq. (2) can be rewritten to include the possibility that the particles' centers lie at different elevations:

$$U_{dip} = -\frac{\mu_0 m^2}{4\pi}\left[\frac{r_{\parallel}^2 - 2z^2}{(r_{\parallel}^2 + z^2)^{5/2}}\right] \ , \tag{5}$$

where now $r_{\parallel}$ and z are respectively the in-plane and the vertical separations between the confined colloids. Eq. (5) shows that, for a field perpendicular to the particle plane, the colloids repel when the difference between the elevation of their centers is $\Delta z < d/\sqrt{5}$, while the potential becomes short-range attractive and long-range repulsive in the other case. This situation allows for attractive interactions to arise, as opposed to the fully confined case.

The other feature is that, instead of using a static, vertical field as in Ref. [38], we use a precessing magnetic field which performs a conical rotation at an angle θ around the $\hat{\boldsymbol{z}}$ axis,

$$\boldsymbol{B} = B_0[\cos\theta\hat{\boldsymbol{z}} + \sin\theta(\cos(2\pi f t)\hat{\boldsymbol{x}} + \sin(2\pi f t)\hat{\boldsymbol{y}})] \ , \tag{6}$$

where the hatted vectors denote the unit vectors of our reference frame, being B_0 the field amplitude and f the driving frequency, Fig. 1(d). As shown in the sequence of images in Fig. 1(a–c) the applied modulation organizes the particles into different dynamic states which arise from the balance between the dipolar interactions, Eq. (5) and the strong hard-wall confinement. Starting from a disordered liquid-like phase, Fig. 1(a), the colloids assemble into localized rotating dimers for $f = 1$ Hz and $\theta = 26.9°$. The two particles composing each dimer are located close to the top and bottom substrate, as shown in the schematics of Fig. 1(b). For relatively low frequencies, the dimers perform synchronous rotation with the precessing field, i.e. the dimer director follows $\boldsymbol{B}$ with a constant phase lag angle. By increasing f to

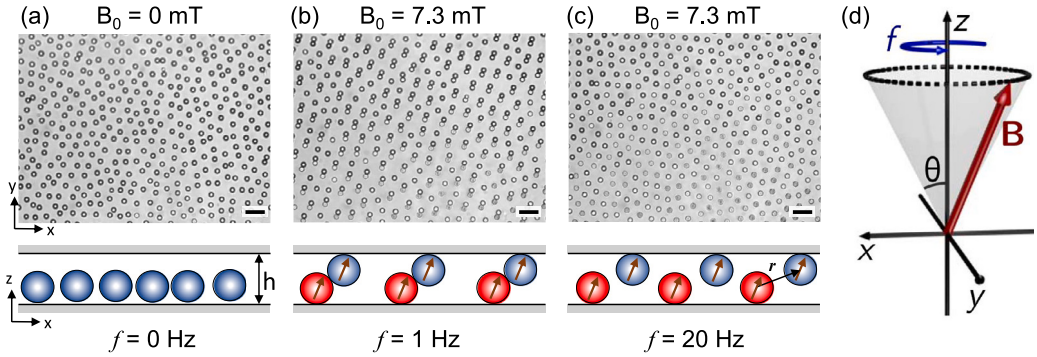

Fig. 1. (a–c) Sequence of experimental images showing a confined layer of paramagnetic colloids in absence of field (a), and with a precessing field with $B_0 = 7.3$mT, $\theta = 27°$ and driving frequency $f = 1$ Hz (b) and $f = 10$ Hz (c). The schematics at the bottom shows the corresponding particle location in the $(\hat{x}, \hat{z})$ plane, being h the cell thickness. Top (bottom) particles are highlighted in blue (red) in the second and third images. The sequence of images at the top has been adapted from Ref. [30], with permission from the American Association for the Advancement of Science's, Copyright [2020]. (d) Sketch of a magnetic field $\boldsymbol{B}$ precessing with an angle θ respect to the $\hat{z}$ axis.

20 Hz the dimers are unable to follow the fast field evolution, and they break up releasing the composing particles that now repel and create two separate lattices made of particles located close to one of the two plates. For the range of field parameters used, the upper and lower particles do not simply switch vertical positions but instead separate remaining each localized along the original plane. This effect occurs because the sign of the interaction between the colloids forming the dimers depends on the angle Δ between the projections of $\boldsymbol{B}$ on the $(\hat{\boldsymbol{x}}, \hat{\boldsymbol{y}})$ plane and the dimer's director (namely, the vector joining the centers of the colloids in the dimer), as described in Ref. [31] and in the Supporting Information of Ref. [30]. At low frequencies, the dimers can rotate phase-locked with the field and Δ remains constant, while at higher frequencies phase slipping occurs and Δ increases within one period up to a critical value Δ_c, where the dipolar force between the particles inside the dimer switches from attractive to repulsive, causing the dimer to break and the colloids to be expelled. During this phase-slipping, the dimers do not change their inclination with respect to the $(\hat{\boldsymbol{x}}, \hat{\boldsymbol{y}})$ plane.

4. Symmetric precessing field: enhanced diffusion

When forcing the system to transit from the dimer (Fig. 1(b)) to the up-down state (Fig. 1(c)) it was experimentally observed that, at large densities, the particles display an intermediate regime where the dimers form and destroy, exchanging the particle position continuously. The basic mechanism of this "exchange" regime is illustrated in the sequence of images in Fig. 2(a) with the accompanying schematics on the right side. Here particles close to the top and bottom plates are respectively colored in blue and red. The exchange process is similar to a "ceilidh"-like dance: free particles of different colors first bind into a rotating dimer for half of the field period due to attractive dipolar interactions, and then they break during the other half period when such interactions become repulsive [31]. In this exchange process "up" or "down" particles remain located in the same plane and move along this plane without changing elevation.

Here we use numerical simulations with a packing fraction $\Psi = 0.3$, to analyze in detail the particle dynamics for both an isotropic precessing field (Fig. 1(d)) and a biased one, as described later. In the first case, the magnetic modulation is spatially isotropic in the $(\hat{x}, \hat{y})$ plane and we observe that the particles continuously form and destroy the dimers by moving across the two planes without showing a preferred direction. Thus, the paramagnetic colloids display trajectories similar to a two dimensional random walk characterized by a constant step length that roughly corresponds to the average interdimer distance. We start characterizing this motion by measuring the distribution of displacements $G(\Delta r, \Delta t)$ which is the self-part of the Van Hove correlation function [39] and gives the probability that a particle undergoes a displacement of magnitude Δr after a time interval Δt. For a standard diffusive process, $G(r, t)$ follows a Gaussian distribution, from which, $G(\boldsymbol{r}, t) = \frac{1}{4\pi Dt} \exp(-\boldsymbol{r}^2/(4Dt))$ being D the two dimensional diffusion coefficient. Effectively, as shown in Fig. 2(b), the distribution of displacements along both directions, Δx and Δy, can be well fitted by a Gaussian function for all time considered. The particle motion is isotropic in the plane as shown by the similarity between the distributions along the two directions. We further calculate from the in-plane particle trajectories $\boldsymbol{r}_i \equiv (x, y)$ the two-dimensional mean squared displacement (MSD), Fig. 2(c). The MSD is computed as $\mathrm{MSD}(\tau) \equiv \langle \Delta r^2(\tau) \rangle = \langle |\boldsymbol{r}(t) - \boldsymbol{r}(t+\tau)|^2 \rangle \sim \tau^\alpha$, where the brackets denote both an ensemble average and a rolling time average on the starting time t. Here α is the exponent of the power law that can be used to distinguish the diffusive dynamics ($\alpha = 1$) from the superdiffusive ($\alpha > 1$) and ballistic ($\alpha = 2$) ones, the latter corresponding to directed particle transport. In particular, we observe that at short time scale $\tau \lesssim 0.1$ s, when the particles jump from one dimer to the next, they move at a constant speed and $\alpha = 2$. In contrast, at longer time $\tau > 10$ s, the motion becomes diffusive and the slope of the MSD reduces to one. In the long time limit, one may extract the two-dimensional effective diffusion coefficient, as $D_{\mathrm{eff}} = \lim_{t\to\infty} \langle \Delta r^2 \rangle / (4t)$. Such quantity is shown in Fig. 2(d) for different driving frequencies, $f \in [3.29, 3.6]$ Hz. We rescale D_{eff} by the corresponding diffusion coefficient previously measured for unconfined magnetic colloids in water, $D_0 = \frac{k_B T}{\gamma} = 0.07\ \mu\mathrm{m}^2\ \mathrm{s}^{-1}$. As shown in Fig. 2(d), in the exchange state the particles display an enhanced diffusive dynamics, where D_{eff} can increase up to 60 times D_0. Eventually D_{eff} should reach a maximum value at large frequencies, as observed in previous works on magnetic particles driven across different structured substrates [40,41], however, we find that by increasing further f the exchange mechanism breaks down as now the particles are unable to jump between the dimers due to viscous damping. Thus, within this range of parameters, a spatially symmetric precessing field produces a tuneable diffusive dynamics which can be controlled by the driving frequency of the precessing field.

5. Bi-directional colloidal current

The enhanced diffusive dynamics are observed for a magnetic modulation which is spatially symmetric in the particle plane. By breaking such symmetry, one can achieve a directed transport in form of a bidirectional current of colloids, as shown in Fig. 3(a), VideoS1 in Supplementary Materials. This was obtained by adding a small tilt angle δ to the precessing field such that it now performs an asymmetric conical motion, Fig. 3(b), given by:

$$\boldsymbol{B}(t) = B_0[(\sin(\theta)\cos(2\pi f t) + \cos(\theta)\sin(\delta))\hat{\boldsymbol{x}} + \sin(\theta)\sin(2\pi f t)\hat{\boldsymbol{y}} + \cos(\theta)\cos(\delta)\hat{\boldsymbol{z}}] \ , \quad (7)$$

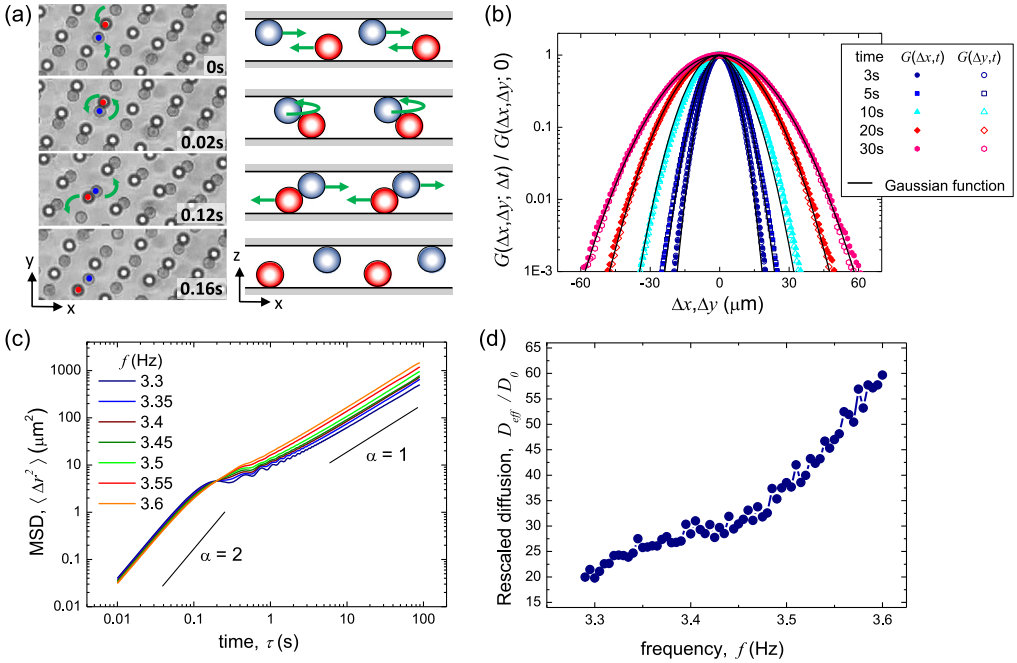

Fig. 2. (a) Experimental images and corresponding schematics showing the exchange process that leads to a net particle transport. Colloids closer to the top plate (blue) are attracted towards those closer to the bottom plate (red), they form a rotating dimer and, after half-field cycle, the dimer breaks releasing the constituting particles. The first column of images has been adapted from Ref. [31], with permission from the American Physical Society, Copyright [2020]. (b) Normalized displacement probability distribution $G(\Delta x, \Delta y; \Delta t)$ calculated along the x (filled symbols) and y (empty symbols) directions at different times for $f = 3.6$ Hz. Continuous black lines are non-linear regressions using a Gaussian function. (c) Two dimensional mean squared displacement $\langle \Delta r^2 \rangle$ versus time t for different frequencies f. In the image are shown the slope of the power law indicating ballistic ($\alpha = 2$) and diffusive ($\alpha = 1$) regimes. (b) Normalized long time effective diffusion coefficient D_{eff} versus frequency f, being D_0 the diffusion of unconfined particles.

which is equivalent introducing an additional bias field along the $\hat{\boldsymbol{x}}$ direction. As a result, the magnetic colloids flow bidirectionally with "up" and "down" pointing particles moving in opposite senses. This current is made of colloids that slide between each other on two parallel planes periodically forming and destroying dimers in a synchronized way, Fig. 3(a). The current can be quantified from the mean particle velocity which is calculated as $\bar{\boldsymbol{v}}_m = \langle (v_{y,i}\hat{\boldsymbol{x}} - v_{x,i}\hat{\boldsymbol{y}}) z_i / |z_i| \rangle$ being z_i the elevation of the particle i characterized by the velocity components $(v_{x,i}, v_{y,i})$. This expression for the velocity appears from taking the vectorial product between the velocity vector, and the unit vector of the height of the particle. Thus, we define the bidirectional current as $I = 2|\bar{\boldsymbol{v}}_m|/(f d\sqrt{\pi/(\sqrt{3}\Psi)})$, being Ψ the normalized particle packing fraction. Since this current is composed of particles sliding along the same direction but opposite senses, to measure its amplitude I we take the absolute value of $\boldsymbol{v}_m$. As defined, I acquires the maximum value of 1 when all particles are mobilized and jump synchronously one lattice constant per field cycle. As shown in Fig. 3(c), the colloidal current can be tuned by varying the different field parameters, being sensitive to both the frequency and the tilt angle. In particular, for $\delta = 10°$ and at low frequency $f < 2.5$ Hz, we observe low values of the current, that decrease and becomes close to zero. In contrast, for larger f the current increases sharply to $\langle I \rangle \sim 1$, and then decreases for $f > 5$ Hz. Increasing δ reduces the threshold value for the current saturation even if the trend is similar, first a sharp rise followed by a slow decrease in amplitude. Varying δ at fixed frequency reveals that I can also increase more smoothly for $f = 6$ Hz, although it shows wider fluctuations around its mean value. In contrast to the experiments performed in [30], where particles can leave or enter the observation area, in our simulation the number of particles is conserved due to periodic boundary conditions along the $(\hat{\boldsymbol{x}}, \hat{\boldsymbol{y}})$ plane. Indeed, we measure the current for an initially even number of particles, such that in the case $I = 1$ all particles from different planes form the dimers during half a period. Thus, we ask whether this transport mechanism is modified when an odd number of colloids is present in the system, meaning that at least one particle is not in a dimer every half period and acts as a defect in the otherwise regular structure. However, this was not the case as shown in Fig. 3(d), where we plot the time evolution of I for both N even (left) and odd (right). In both situations, the system shows similar dynamic states where I reaches a maximum value for large tilt angles $\delta > 20°$ and displays a similar reduction in amplitude for smaller δ, vanishing in the isotropic case, $\delta = 0°$. Thus, the bidirectional current represents a rather robust way to transport matter at the micrometer scale, and can be fully controlled via the precessing field, with an increasing amplitude with the induced spatial anisotropy, here given by the tilt angle δ.

6. Breaking transport: magnetic "holes".

The maximum bidirectional colloidal current can be achieved under relatively large tilt angles $\delta > 10°$, (Fig. 3(d)) independently from the presence of single defects introduced by changing the ratio of "up" and "down" particles. Thus, we consider "stronger" defects placed in a controlled amount, such that they could dramatically influence the sliding process. We introduce in our system magnetic "holes", namely colloidal particles capable of acquiring an induced moment along the opposite direction of an applied field. In the field of colloidal science, these "holes" can be realized by immersing non magnetic particles in a ferrofluid matrix, as originally proposed by Skjeltorp [42,43] and later exploited in several subsequent works [28,44–49]. When immersed in a magnetizable fluid, a spherical particle of radius a under an external field $\boldsymbol{B}$ acquires an induced moment $\boldsymbol{m} = 4\pi a^3 \Delta\chi \boldsymbol{B}/\mu_0$, where the factor $\Delta\chi = (\chi_p - \chi_m)/(\chi_p - 2\chi_m + 3)$ contains the magnetic susceptibilities of both, the particle χ_p and the dispersing medium χ_m [47]. It was previously shown that there are ferrofluids capable of hosting both paramagnetic (χ_{pm}) and non magnetic (χ_p) particles and featuring a susceptibility value between that of the two particles, $\chi_p < \chi_m < \chi_{pm}$. Under an external field $\boldsymbol{B}$, the paramagnetic and non magnetic colloids will have both induced point dipoles, but the first will align along the field direction and the last antiparallel to it, as shown in the schematics in Fig. 4(a). Note that the dipolar interaction energy

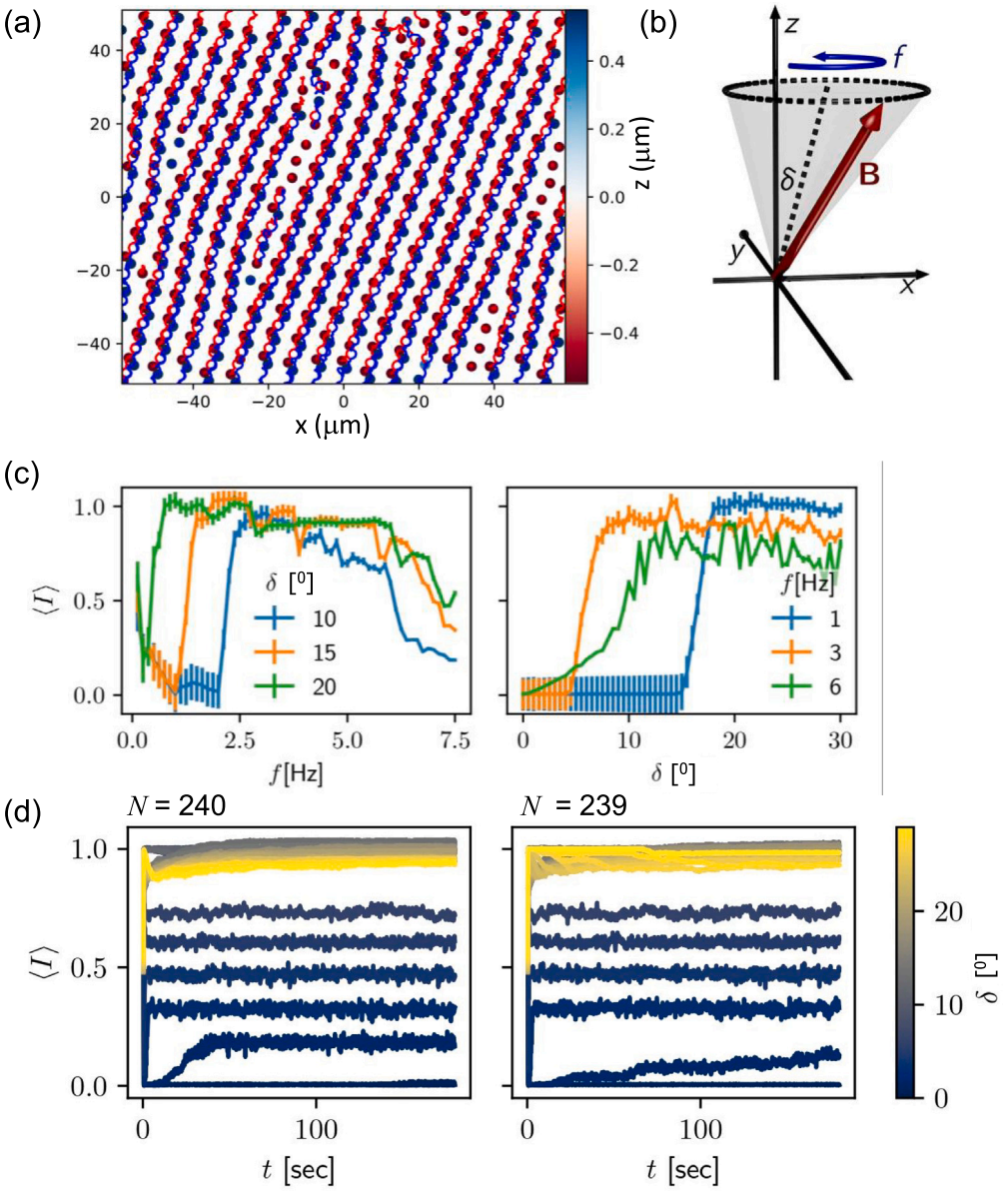

Fig. 3. (a) Simulation snapshot illustrating the particle positions colored based on their elevation z (legend on the side) with their trajectories superimposed. Simulation parameters are $B = 7.2mT$, $\theta = 26.9°$, $f = 6$ Hz, $\delta = 7°$, the cell thickness is $h = 4$ μm, and packing fraction $\Psi = 0.35$. (b) Schematic showing the biased precessing magnetic field described by Eq. (7) with a tilt angle δ. (c) Average current $\langle I \rangle$ versus frequency f (left) and tilt angle δ (right). (d) Average current $\langle I \rangle$ as a function of time for different values of δ, legend on the side, for a system with an even number particles (left) and an odd N, right.

$U_{dip}(\boldsymbol{m}_i, \boldsymbol{m}_j, \boldsymbol{r})$ and respective force $F_{dip}(\boldsymbol{m}_i, \boldsymbol{m}_j, \boldsymbol{r})$ change sign when one of the two moments is inverted, $U_{dip}(\boldsymbol{m}_i, -\boldsymbol{m}_j, \boldsymbol{r}) = -U_{dip}(\boldsymbol{m}_i, \boldsymbol{m}_j, \boldsymbol{r})$ and $F_{dip}(\boldsymbol{m}_i, -\boldsymbol{m}_j, \boldsymbol{r}) = -F_{dip}(\boldsymbol{m}_i, \boldsymbol{m}_j, \boldsymbol{r})$, meaning that particles with antiparallel moments attract when those with parallel ones repel and vice-versa. Thus, we have tested how the presence of these "magnetic holes" may influence the particle current considering the initial, ideal situation of a lattice made of N paramagnetic colloids and a fraction Φ of non-magnetic particles in an host medium having χ_m. We investigate this system performing simulations similar to the previous one, with a packing fraction $\Psi = 0.2$, and $N_d = N\Phi$ non-magnetic particles in the ferrofluid by assigning to N_d of our particles a negative susceptibility $\chi_d < 0$.

In particular, we consider the effective susceptibility of the non-magnetic particles to be exactly the opposite of that of the paramagnetic ones, namely $\chi_d = -0.4$. Furthermore, to avoid creating artifacts such as particle segregation at the start of the simulation, we start from colloids arranged in dimers whose centers form a triangular lattice, and, from this arrangement, we randomly select the N_d particles with negative susceptibility.

We find that already the presence of one inclusion is able to dramatically change the particle current. For a system that would have bidirectional sliding along the $\hat{\boldsymbol{x}}+\hat{\boldsymbol{y}}$ direction, the inclusion, highlighted with a green circle in Fig. 4(b), breaks the particle flow along one line, creating a series of defects in the form of unpaired colloids. The hole also attracts approaching particles from both planes, forming a cluster that temporarily produces local jamming, as shown in the sequence of images in Fig. 4(c). In this image we also illustrate the Voronoi tessellation for the case of one magnetic hole and for a driving frequency of 3 Hz. After ∼100 field cycles, the hole is able to induce several defects along the direction of the current and destroy the order of the dimer lattice without having moved too much from its starting position. The number of clusters increase with the fraction of magnetic holes and for $\Phi = 0.25$ we find that the bidirectional current almost vanishes while most of the particles located close to the top plate are attracted by the defect, leaving the particles of the bottom plate (red) free to

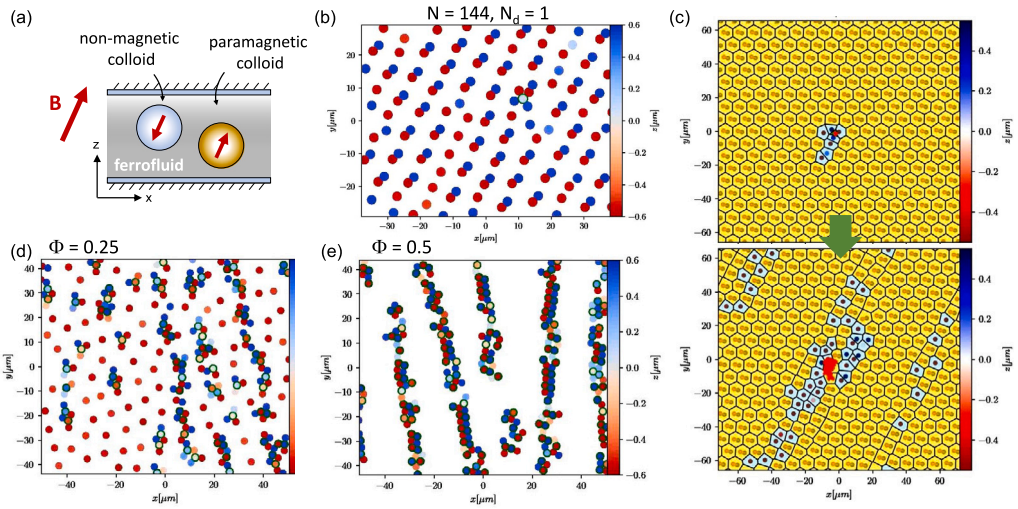

Fig. 4. (a) Scheme of the direction of the induced moments within a paramagnetic (yellow) and a non-magnetic (blue) colloid that are both dispersed in a ferrofluid and subjected to an external magnetic field $\boldsymbol{B}$. (b) Snapshot showing the particle arrangements at the steady state for one "magnetic hole", see VideoS2 in Supplementary Materials. (c) Dimer order for one "hole", $N = 612$ particles and driving frequency $f = 3$ Hz at two different instants of time: $t = 1T = 0.33$s (top) and after $t = 111T = 37$s (bottom) being $T = 1/f$ the period of the biased precessing field. The two images show the Voronoi tessellation where cells in yellow contain dimers (which are identified when two colloids are closer than a threshold distance approximately equal to their diameter) and light blue colored cells contain isolated particles. The red dot in the top image represents the starting position of the "magnetic hole" at $t = 1T$ and its trajectory up to $t = 111T$ is displayed as a red line in the bottom image. (d,e) Simulation snapshots showing the arrangement of a total of $N = 288$ particles for different fractions Φ of "magnetic holes": (d) $\Phi = 0.25$, VideoS3 in Supplementary Materials and (e) $\Phi = 0.5$, VideoS4 in Supplementary Materials. In all images the particles are colored based on their elevation (legend on the side of the images) and the defects or "magnetic holes" are highlighted with a green circle.

perform localized diffusive motion, Fig. 4(d). The clusters break the colloidal current since, by attracting particles they induce fluctuations in the density of the system, breaking down the pathways along which the current flowed and destroying the exchange mechanism. At steady state, these clusters tend to organize into parallel chains along the $\hat{\boldsymbol{y}}$ direction favoring particle exchange along this direction. In the extreme case of equal number of defects and paramagnetic colloids, $\Phi = 0.5$ and Fig. 4(e), we observe that both types of particles organize into parallel lines along the $\hat{\boldsymbol{y}}$ direction, that is perpendicular to the bias direction, where colloids slides laterally between each other showing a dynamical regime similar to an edge current observed for rotating magnetic clusters [50,51]. By increasing further Φ the dynamical scenario inverts since now the paramagnetic colloids behave as defects and the current can be fully restored when the fraction of these particles reduces to zero.

7. Conclusions

We have shown that it is possible to induce enhanced diffusive dynamics or bi-directional flow in an ensemble of paramagnetic colloids when confined in a thin cell and subjected to external, time dependent field modulations. The difference between random particle excursion and directed transport arises from the presence of a small tilt angle that breaks the spatial symmetry of the precessing field introducing a preferred direction of motion, perpendicular to the applied bias. Moreover, the current can be easily destabilized by introducing defects in form of "magnetic-holes", i.e. non-magnetic particles dispersed within a ferrofluid carrier.

Our numerical work could be further extended along different directions. For example one could investigate more the effect of the defects and whether it is possible to selectively control them in order to regulate the particle flow. Further, the fact that the bidirectional current rises step wise or continuously for different values of the control parameters may be investigated in order to understand the role of fluctuations at the transition point and whether this type of non-equilibrium transition shows signatures of first or second order. Also plans to introduce different types of attractive interactions as those arising from the presence of a dispersed polymer, i.e. depletion interactions, are on the way.

CRediT authorship contribution statement

Mattia Ostinato: Data curation, Formal analysis, Investigation, Resources, Software, Validation, Writing – review & editing. **Antonio Ortiz-Ambriz:** Data curation, Formal analysis, Methodology, Supervision, Validation. **Pietro Tierno:** Conceptualization, Formal analysis, Funding acquisition, Project administration, Supervision, Writing – original draft, Writing – review & editing.

Declaration of competing interest

The authors declare that they have no known competing financial interests or personal relationships that could have appeared to influence the work reported in this paper.

Data availability

Data will be made available on request.

Acknowledgments

We thank Charles Reichhardt, Andras Libal and Cristiano Nisoli for stimulating discussions on the edge current. This work has received funding from the European Research Council (ERC) under the European Union's Horizon 2020 Research and Innovation Programme (grant agreement no. 811234). We also thank the Ministerio de Ciencia, Innovación *y* Universidades (grant no. PID2022-137713NB-C21 AEI/FEDER-EU) and the Agència de Gestió d'Ajuts Universitaris i de Recerca (project 2021 SGR 00450). P.T. support from the Generalitat de Catalunya (ICREA Académia).

Appendix A. Supplementary data

Supplementary material related to this article can be found online at https://doi.org/10.1016/j.jmmm.2023.171701.

References

[1] P. Reimann, Brownian motors: Noisy transport far from equilibrium, Phys. Rep. 361 (2002) 57.
[2] P. Hänggi, F. Marchesoni, Artificial brownian motors: Controlling transport on the nanoscale, Rev. Modern Phys. 81 (2009) 387–442.
[3] N. Pamme, Recent advances and current challenges in magnetophoresis based micro magnetofluidics, Magn. Microfluid. 6 (2006) 24–38.
[4] P. Tierno, Depinning and collective dynamics of magnetically driven colloidal monolayers, Phys. Rev. Lett. 109 (2012) 198304.
[5] C. Reichhardt, C.J.O. Reichhardt, Depinning and nonequilibrium dynamic phases of particle assemblies driven over random and ordered substrates: a review, Rep. Progr. Phys. 80 (2) (2016) 026501.
[6] M. Urbakh, J. Klafter, D. Gourdon, J. Israelachvili, The nonlinear nature of friction, Nature 430 (2004) 525–528.
[7] A. Vanossi, N. Manini, M. Urbakh, S. Zapperi, E. Tosatti, Colloquium: Modeling friction: From nanoscale to mesoscale, Rev. Modern Phys. 85 (2013) 529–552.
[8] J. Yan, M. Bloom, S.C. Bae, E. Luijten, S. Granick, Linking synchronization to self-assembly using magnetic janus colloids., Nature 491 (2012) 578–581.
[9] M.P. Juniper, A.V. Straube, R. Besseling, D.G.A.L. Aarts, R.P. Dullens, Microscopic dynamics of synchronization in driven colloids, Nature Commun. 6 (2015) 7187.
[10] P.T. Korda, M.B. Taylor, D.G. Grier, Kinetically locked-in colloidal transport in an array of optical tweezers, Phys. Rev. Lett. 89 (2002) 128301.
[11] T. Bohlein, C. Bechinger, Experimental observation of directional locking and dynamical ordering of colloidal monolayers driven across quasiperiodic substrates, Phys. Rev. Lett. 109 (2012) 058301.
[12] R.L. Stoop, A.V. Straube, T.H. Johansen, P. Tierno, Collective directional locking of colloidal monolayers on a periodic substrate, Phys. Rev. Lett. 124 (2020) 058002.
[13] C.M. Pooley, G.P. Alexander, J.M. Yeomans, Hydrodynamic interaction between two swimmers at low reynolds number, Phys. Rev. Lett. 99 (2007) 228103.
[14] E. Lauga, T.R. Powers, The hydrodynamics of swimming microorganisms, Rep. Progr. Phys. 72 (2009) 096601.
[15] K. Drescher, K.C. Leptos, I. Tuval, T. Ishikawa, T.J. Pedley, R.E. Goldstein, Dancing *Volvox* : Hydrodynamic bound states of swimming algae, Phys. Rev. Lett. 102 (2009) 168101.
[16] K. Schaar, A. Zöttl, H. Stark, Detention times of microswimmers close to surfaces: Influence of hydrodynamic interactions and noise, Phys. Rev. Lett. 115 (2015) 038101.
[17] R.S. Molday, S.P.S. Yen, A. Rembaum, Application of magnetic microspheres in labelling and separation of cells, Nature 268 (1977) 437–438.
[18] C.T. Yavuz, A. Prakash, J. Mayo, V.L. Colvin, Magnetic separations: From steel plants to biotechnology, Chem. Eng. Sci. 64 (10) (2009) 2510–2521.
[19] J.L. Corchero, A. Villaverde, Biomedical applications of distally controlled magnetic nanoparticles, Trends Biotechnol. 27 (2009) 468.
[20] A. Munaz, M.J.A. Shiddiky, N.-T. Nguyen, Recent advances and current challenges in magnetophoresis based micro magnetofluidics, Biomicrofluidics 12 (2018) 031501.
[21] Magnetophoresis in microfluidic lab: Recent advance, Sensors Actuators A 332 (2021) 113180.
[22] T.B. Jones, Electromechanics of Particles, Cambridge University Press, Cambridge; United Kingdom, 2009.
[23] J.Y. Hwang, M. Takayasu, F.J. Friedlaender, G. Kullerud, Application of magnetic susceptibility gradients to magnetic separation, J. Appl. Phys. 55 (1984) 2592–2594.
[24] M. Zborowski, J.J. Chalmers, Magnetophoresis: Fundamentals and Applications, John Wiley & Sons, Ltd, 2015.
[25] Q. Ramadan, V. Samper, D. Poenar, C. Yu, On-chip micro-electromagnets for magnetic-based bio-molecules separation, J. Magn. Magn. Mater. 281 (2) (2004) 150–172.
[26] E. Mirowski, J. Moreland, A. Zhang, S.E. Russek, M.J. Donahue, Manipulation and sorting of magnetic particles by a magnetic force microscope on a microfluidic magnetic trap platform, Appl. Phys. Lett. 86 (24) (2005) 243901.
[27] K. Gunnarsson, P.E. Roy, S. Felton, J. Pihl, P. Svedlindh, S. Berner, H. Lidbaum, S. Oscarsson, Programmable motion and separation of single magnetic particles on patterned magnetic surfaces, Adv. Mat. 17 (2005) 1730–1734.
[28] B.B. Yellen, O. Hovorka, G. Friedman, Arranging matter by magnetic nanoparticle assemblers, Proc. Natl. Acad. Sci. USA 102 (2005) 8860–8864.
[29] P. Tierno, F. Sagués, T.H. Johansen, T.M. Fischer, Colloidal transport on magnetic garnet films, Phys. Chem. Chem. Phys. 11 (2006) 9615–9625.
[30] H. Massana-Cid, A. Ortiz-Ambriz, A. Vilfan, P. Tierno, Emergent collective colloidal currents generated via exchange dynamics in a broken dimer state, Sci. Adv. 6 (2020) eaaz2257.
[31] F. Meng, A. Ortiz-Ambriz, H. Massana-Cid, A. Vilfan, R. Golestanian, P. Tierno, Field synchronized bidirectional current in confined driven colloids, Phys. Rev. Res. 2 (2020) 012025.
[32] S. Plimton, Fast parallel algorithms for short-range molecular dynamics, J. Comput. Phys. 117 (1995) 1–19.
[33] M. Puljiz, S. Huang, K.A. Kalina, J. Nowak, S. Odenbach, M. Kästner, G.K. Auernhammer, A.M. Menzel, Reversible magnetomechanical collapse: virtual touching and detachment of rigid inclusions in a soft elastic matrix, Soft Matter 14 (2018) 6809–6821.
[34] E. Allahyarov, H. Löwen, L. Zhu, Dipole correlation effects on the local field and the effective dielectric constant in composite dielectrics containing high-: K inclusions, Phys. Chem. Chem. Phys. 18 (2016) 19103–19117.
[35] K. Zahn, R. Lenke, G. Maret, Two-stage melting of paramagnetic colloidal crystals in two dimensions, Phys. Rev. Lett. 82 (1999) 2721–2724.
[36] K. Mangold, P. Leiderer, C. Bechinger, Phase transitions of colloidal monolayers in periodic pinning arrays, Phys. Rev. Lett. 90 (2003) 158302.
[37] C. Eisenmann, U. Gasser, P. Keim, G. Maret, Anisotropic defect-mediated melting of two-dimensional colloidal crystals, Phys. Rev. Lett. 93 (2004) 105702.
[38] N. Osterman, D. Babič, I. Poberaj, J. Dobnikar, P. Ziherl, Observation of condensed phases of quasiplanar core-softened colloids, Phys. Rev. Lett. 99 (2007) 248301.
[39] L. Van Hove, Correlations in space and time and born approximation scattering in systems of interacting particles, Phys. Rev. 95 (1954) 249–262.
[40] P. Tierno, P. Reimann, T.H. Johansen, F. Sagués, Giant transversal particle diffusion in a longitudinal magnetic ratchet, Phys. Rev. Lett. 105 (2010) 230602.
[41] R.L. Stoop, A.V. Straube, P. Tierno, Enhancing nanoparticle diffusion on a unidirectional domain wall magnetic ratchet, Nano Lett. 19 (2019) 433.
[42] A.T. Skjeltorp, One- and two-dimensional crystallization of magnetic holes, Phys. Rev. Lett. 51 (1983) 2306–2309.
[43] A.T. Skjeltorp, Monodisperse particles and ferrofluids: a fruit-fly model system, J. Magn. Magn. Mater. 65 (2020) 195–203.
[44] P. Pieranski, S. Clausen, G. Helgesen, A.T. Skjeltorp, Braids plaited by magnetic holes, Phys. Rev. Lett. 77 (1996) 1620–1623.
[45] J. Černák, G. Helgesen, Aggregation of magnetic holes in a rotating magnetic field, Phys. Rev. E 78 (2008) 061401.
[46] G. Helgesen, P. Pieranski, A.T. Skjeltorp, Nonlinear phenomena in systems of magnetic holes, Phys. Rev. Lett. 64 (1990) 1425–1428.
[47] R.M. Erb, H.S. Son, B. Samanta, V.M. Rotello, B.B. Yellen, Magnetic assembly of colloidal superstructures with multipole symmetry, Nature 457 (2009) 999–1002.
[48] A. Ray, T.M. Fischer, Magnetic field controlled composite paramagnetic–diamagnetic colloidal phases, J. Phys. Chem. B 116 (2012) 8233–8240.
[49] J. Loehr, M. Loenne, A. Ernst, D. de Las Heras, T.M. Fischer, Topological protection of multiparticle dissipative transport, Nature Commun. 7 (2016) 11745.
[50] J. Yan, S.C. Bae, S. Granick, Rotating crystals of magnetic janus colloids, Soft Matter 11 (2015) 147–153.
[51] H. Massana-Cid, D. Levis, R.J.H. Hernández, I. Pagonabarraga, P. Tierno, Arrested phase separation in chiral fluids of colloidal spinners, Phys. Rev. Res. 3 (2021) L042021.